RESEARCH ON A CO2 RECOVERY SYSTEM FROM INDUSTRIAL FLUE GAS BY SOLID ADSORPTION VIA DUAL-COLUMN ALTERNATING TSA CYCLES

Phạm Văn Cảnh*, Lê Thị Thuý Vy, Bùi Hệ Thống

Faculty of Mechanical Engineering, The University of Danang - University of Technology and Education

**Corresponding author: Phạm Văn Cảnh (23115041122205@sv.ute.udn.vn)*

Abstract—This study presents a coupled thermal-adsorption-regeneration simulation of a dual-column TPSA system using zeolite 13X for CO2 recovery from industrial flue gas. Three simulation cases were investigated: (A) transient thermal analysis of the column-heating assembly in ANSYS Transient Thermal; (B) transient CFD adsorption in ANSYS Fluent for an inlet stream containing 15% CO2 to obtain concentration fields, flow pathlines, and the breakthrough curve; and (C) time-dependent regeneration under simultaneous wall heating and outlet vacuum to evaluate the regeneration behaviour of the packed bed. Case A shows that the maximum temperature rapidly reaches about 576,71 K, whereas the bed-average temperature and especially the coldest region increase much more slowly; at 1800s, the system-average temperature is about 392,43 K. Case B indicates that the adsorption front moves from the top toward the bottom of the column and that the outlet CO2 concentration remains nearly zero until approximately 1350s before rising sharply. In case C, the average adsorption loading decreases from about 0,198 to nearly the residual value of 0,005, while the final contour confirms a nearly uniform regeneration state throughout the bed. These results demonstrate that the A-B-C simulation chain is suitable for determining switching time, regeneration time, and guiding the optimization of a laboratory-scale dual-column TPSA system.

Keywords—TSA, zeolite 13X, Ansys Fluent, Transient Thermal, breakthrough, Linear Driving Force (LDF), CO_2 capture.

I. INTRODUCTION

Industrial post-combustion flue gas from typical coal-fired sources contains CO2 at 12 - 15% by volume near atmospheric pressure, making CO2 separation challenging because of the low separation driving force and the energy cost of CO2 recovery/compression [1]. In reviews of CO2 capture technologies, adsorption using molecular sieves/activated carbon and desorption by PSA or TSA have been recognized as one possible approach; however, TSA has generally received less attention than PSA for flue gas because of its long cycle time (heating the packed bed) and the need to shorten the "unused bed length" through rapid cycling [2].

Zeolite 13X is described as having an effective pore size of ~10 Å and a high adsorption capacity; it is also a commercial material widely used in PSA/TSA processes [3]. However, the influence of water vapor is an important bottleneck: breakthrough data show that under humid conditions, zeolite 13X gradually becomes saturated with water, reducing CO2 capacity over successive cycles and requiring a higher activation temperature for complete reactivation [4].

Moisture management in the fabricated prototype is addressed as follows: because zeolite 13X is highly sensitive to water vapor, the prototype includes an inlet pre-treatment train composed of a particulate filter, a condensate trap/cooler, and a drying cartridge filled with silica gel or a dry molecular sieve before the gas reaches the adsorption column. Before each test, the zeolite bed is thermally reactivated and the gas lines are purged with dry air. During operation, condensate is periodically drained and inlet humidity is checked so that the adsorption tests are performed under a low-moisture condition. This strategy is intended to suppress competitive adsorption of H2O and to improve the repeatability of the CO2 breakthrough behaviour.

A practical gap at the fabricated-model/experimental scale is the lack of manuscripts with a clearly linked heating-adsorption-regeneration simulation sequence and sufficiently detailed Transient Thermal and CFD/porous/UDF settings for reproducibility. Therefore, the objectives of this study are to: build a dual-column alternating TSA system model and a heat-regeneration loop for CO2 recovery [2]; implement simulations A-B-C in Transient Thermal and Ansys Fluent using an isotherm-LDF model and species/energy source terms, with a save/restart procedure for cyclic simulation [5]; and propose an evaluation framework (breakthrough times, dynamic capacity, regeneration energy, and SEC) together with a recommended regeneration operating range of 90-110°C for dry gas, while also noting the 200-300°C range when deep regeneration/dehumidification is required according to molecular sieve technical guidance [6].

A. Principle of dual-column TSA and significance of cycle time

In a dual-column TSA system, one column operates in adsorption mode while the other operates in regeneration mode. After a certain operating period, the switching valve assembly is opened/closed to exchange the functions of the two columns. This configuration allows nearly continuous treatment of the flue-gas stream while reducing waiting time compared with a single-column system [2].

In principle, a TSA cycle consists of three basic phases: adsorption at low temperature; heating–desorption at a higher temperature; and cooling before returning to the adsorption phase. For the problem considered in this study, the inlet gas for case B is set to contain 15% CO2, whereas case C uses thermal conditions to reduce the equilibrium capacity, causing CO2 to leave the zeolite and exit in the regeneration stream.

B. Equilibrium isotherms: Langmuir and Toth, selection of the main model

Langmuir is the classical monolayer model, commonly used to describe physical adsorption under the assumption of a homogeneous surface (in practice, it can be extended to multiple temperatures).

Toth is a semi-empirical model that accounts for surface heterogeneity; multi-temperature CO_2 data on zeolite 13X show that Toth fits well over a wide range (293,15 - 393,15K; up to 2 MPa), and in one study Toth had the lowest average relative error ($\delta \approx 8{,}57\%$) compared with Langmuir-Freundlich and Langmuir.

Because the objective of the TSA simulation involves temperature variation, the paper selects Toth as the main model. A multi-temperature Toth form is presented in the experimental literature together with fitted parameters [7]:

$$q^*(p,T) = \frac{q_m\, p}{(b(T) + p^{n_T})^{1/n_T}}$$

$$b(T) = b_{0T} \exp\left(-\frac{n_T\, \Delta H}{R\, T}\right)$$

For this model, the suggested reference Toth parameter set for CO_2/13X (from multi-temperature data) is:

$q_m = 6{,}437$ mol/kg, $b_{0T} = 576{,}902$ Pa^{-n}, $n_T = 0{,}464$, $\Delta H = 31864{,}04$ J/mol.

In addition, classical high-pressure data also show that CO_2 on 13X can be fitted by Toth/multisite Langmuir, with an isosteric heat of adsorption significantly higher than that of CH_4/N_2, reflecting the strong affinity of CO_2 [8].

C. Adsorption kinetics: the LDF model

The LDF (Linear Driving Force) kinetics model is commonly used in adsorption-column simulation because it is simple and "works well" in predicting dynamic column data and process design thanks to the averaging effect in the column and porous material [9]:

$$\frac{dq}{dt} = k_{\text{LDF}}(q^*(p_{CO2}, T) - q)$$

q: adsorption loading in the porous cell (mol/kg_ads)

k_{LDF}: kinetic constant (s^{-1}), to be adjusted by fitting the breakthrough curve or taken from the literature.

D. Mass balance for CO2 in the column (CFD/porous modeling form)

In Fluent, species transport is solved by a convection-diffusion equation in terms of mass fraction Y_i, and a source/sink term can be added to describe adsorption [10].

General form (model meaning):

$$\frac{\partial(\rho Y_{CO2})}{\partial t} + \nabla \cdot (\rho \vec{v} Y_{CO2}) = \nabla \cdot (\rho D_{\text{eff}} \nabla Y_{CO2}) + S_{CO2}$$

where S_{CO2} is a sink (during adsorption) or a source (during desorption), implemented through a UDF in the porous zone.

E. Heat transfer (Equation of Energy) and heat of adsorption

For case A and for non-isothermal adsorption/desorption simulations, the temperature field is governed by the energy equation in enthalpy form. In the solid domain, this can be written as the transient heat-conduction equation $\rho c_p . \frac{\partial T}{\partial t} = \nabla \cdot (k\, \nabla T) + Q$, where Q is the volumetric heat source. In this study, Q is negligible in most of the domain and the thermal load is introduced through a prescribed temperature boundary condition on the heating-loop region [11], [15].

Heat loss to the surroundings is represented by the convective boundary condition $-k . \frac{\partial T}{\partial n} = h(T_s - T_\infty)$, where h is the convection coefficient, T_s is the surface temperature, and T_∞ is the ambient temperature. When adsorption/ desorption is coupled with temperature variation, the thermal source term associated with the heat of adsorption is commonly written as:

$$S_E = -(1-\varepsilon)\rho_s\, \Delta H_{ads}\, \frac{dq}{dt}$$

ΔH The negative sign denotes exothermic adsorption under the convention $\Delta H_{ads} > 0$. In the present work, this source term is used to interpret the thermal trend of the bed, whereas case A is mainly governed by conduction inside the column assembly and by convective heat exchange with the environment [7], [15].

F. Pressure drop and the Ergun model for the packed bed, linked to porous inputs in Fluent

Fluent allows "Using the Ergun Equation to Derive Porous Media Inputs for a Packed Bed" and emphasizes that the resistance coefficients are commonly based on superficial velocity [12].

The classical Ergun equation (with the original constants 150 and 1,75) is commonly written as:

$$\frac{\Delta P}{L} = \frac{150(1-\varepsilon)^2}{\varepsilon^3}\frac{\mu v_s}{d_p^2} + \frac{1{,}75(1-\varepsilon)}{\varepsilon^3}\frac{\rho v_s^2}{d_p}$$

The constants (150; 1,75) are referred to as the "original form" in studies on the limits of applicability and adjustments according to material, roughness, and particle shape [13].

II. MODEL DESIGN AND SIMULATION NUMERICAL

A. Model design

The zeolite bed in the adsorption column has an inner diameter D = 63 mm and a bed height H = 180 mm. The geometric bed volume is calculated as: V_bed = $\pi D^2 H/4$ = 5.61×10^{-4} m^3. With a packing bulk density of about 700 kg/m^3, the amount of material contained in the column is approximately 0.39 kg.

The source gas in this study is modeled as industrial flue gas with an inlet CO2 composition of 15% by volume; the remainder is mainly air. Column 1 operates in the adsorption phase, while column 2 operates in the thermal regeneration phase. In terms of equipment, the system includes two columns, switching valves, a fan/purge loop, and a heating loop.



Fig.1 3D design model and fabricated prototype

A1. Parameters for this research

Table 1. Numerical simulation

Group	Parameter	Symbol	Proposed investigation range	Value used in simulation	Source/ reference note
Geometry	Column D	D	Fixed	0,063m	Based on the fabricated model
	Bed height H	H	0,12 - 0,30m	0,18m	Sensitive to MTZ, ΔP
	Bed volume	V_{bed}	—	5,61 ×10⁻⁴ m³	Calculated from D, H
Material	Bulk density	ρ_{bulk}	655 - 700 kg/m³	700 kg/m³	Beads 1,6 - 2,5 mm (BASF) [3]
	Porosity bed	ε	0,35 - 0,45	0,4	Must be specified in the porous zone; recommended to verify by mass weighing
	Particle size	d_p	1,6 - 2,5 mm	1,6	Bead size (BASF) [3]
Inlet stream (B)	Inlet CO_2	$y_{CO2,in}$	0,1 - 0,2	0,15	Simulated according to the assignment; typical coal flue gas 10 - 15% [1]
	Inlet velocity	v_{in}	1 - 2 m/s	1,5 m/s	Recommended based on ΔP/Ergun and breakthrough time
	Inlet temperature	T_{in}	293 - 308 K	300 K	Depending on experimental conditions
Kinetics	LDF constant	k_{LDF}	0,01 - 0,2 s⁻¹	0,01 -0,2 s⁻¹	Must be fitted to breakthrough; LDF is suitable for column simulation [9]
Isotherm	Main model	—	—	Toth	Toth gives the best fit, δ≈8,57% [7]
A/C regeneration	Regeneration temperature	T_{des}	560 - 580 K (dry gas)	Reach 573,15K (~300°C) at 10 minutes	Many studies select 80 - 120°C for CO_2 desorption, 200 - 300°C range when deep regeneration/ dehumidification [6]

A2. Detailed calculation formulas for each case

1. *General formulas for sizing and cycle indicators*

Working capacity:

$$\Delta q_{work} = q^*(p_{ads}, T_{ads}) - q^*(p_{des}, T_{des})$$

Adsorbent mass from the CO2 capture requirement (preliminary design) [14].

$$m_{ads} = \frac{n_{cap}}{\Delta q_{work}}$$

Regeneration energy:

$$E_{reg} = \int_0^{t_{reg}} P_{heater}\,(t)\,dt$$

SEC (Specific Energy Consumption):[2]

$$SEC = \frac{E_{reg}}{m_{CO2,rec}}$$

2. *Case A: Transient thermal analysis (or unsteady-state analysis)*

Unsteady heat conduction equation in solids [15].

$$\rho c_p . \frac{\partial T}{\partial t} = \nabla \cdot (k\,\nabla T) + Q$$

where ρ is the material density, cp is the specific heat, k is the thermal conductivity, T is temperature, t is time, and Q is the volumetric heat source. In the model of this paper, Q = 0 in most of the solid domain; the heating effect is introduced through a prescribed temperature boundary condition on the heating-loop region.

On surfaces exchanging heat with the environment, the convective boundary condition is defined by [15]:

$$-k . \frac{\partial T}{\partial n} = h(T_s - T_\infty)$$

Where $\frac{\partial T}{\partial n}$ is the temperature gradient in the surface-normal direction, T_s is the object surface temperature, and T_∞ is the temperature of the fluid far from the surface

3. *Case B: Time-dependent CO2 adsorption*

4. Breakthrough and dynamic-capacity integration

Definition of breakthrough times:

$$t_{0,05}: \frac{C_{out}}{C_{in}} = 0{,}05; \quad t_{0,50}: \frac{C_{out}}{C_{in}} = 0{,}5;$$

$$t_{0,95}: \frac{C_{out}}{C_{in}} = 0{,}95$$

Integral of the retained CO_2 amount (from breakthrough):

$$n_{ads} = \int_0^{t_{end}} \left(\dot{n}_{CO2,in} - \dot{n}_{CO2,out}\right) dt$$

$$q_{dyn} = \frac{n_{ads}}{m_{ads}}$$

In experiments, the method for calculating capacity from the difference in concentration over time is also described in breakthrough/dynamic-isotherm experiments [16].

5. Case C: Regeneration and CO2 recovery

Recovered CO2 amount:

$$n_{rec} = \int_0^{t_{reg}} \dot{n}_{CO2,out}\,(t)\,dt$$

Purity (CO2 product purity):

$$Purity = \frac{\int \dot{n}_{CO2,out}\,dt}{\int \dot{n}_{tot,out}\,dt}$$

Recovery (recovery ratio):

$$Recovery = \frac{n_{rec}}{n_{ads}}$$

In terms of cyclic operability, a dual-column TVSA system using zeolite 13X has shown that desorbed CO2 can exceed 90% purity and that the material remains stable after 100 cycles [17].

B. ANSYS simulation setup for A–B–C

B1. General configuration

The computational domain was built from the 3D geometry of the adsorption column and its distributor chambers. In case A, the Transient Thermal model includes the column shell, end caps, zeolite bed, and auxiliary solid parts; in cases B and C, the Fluent domain contains the distributor chamber, the porous zeolite bed, and the inlet/outlet boundaries.

Cases B and C were solved with the pressure-based transient solver. Gas composition was described by species transport with CO_2 as the tracked component, while the zeolite layer was modeled as porous media with prescribed porosity and resistance coefficients. Adsorption loading was stored in a UDS, and the LDF-based adsorption/desorption rate was introduced through source terms.

To maintain continuity among the three analyses, geometry and material parameters were kept consistent across the workflow. The zeolite bed had D = 0,063 m, H = 0,18 mm, porosity of about 0,4 , and bulk density of roughly 700 kg/m³. Case/data files were stored by time step to allow restart and post-processing of each stage.

B2. Case A: Transient thermal analysis (or unsteady-state analysis) in Transient Thermal

Case A was defined to evaluate heat transfer from the heater region to the column body and packed bed. The initial uniform temperature was 298,15 K. A prescribed thermal load was applied on the heater region according to the schedule 298,15 K at t = 0s, increased to 573,15 K at 30s, then maintained up to 600s and then stop heating. External surfaces exchanged heat with the surroundings at T_∞ = 298,15 K; the convection coefficient was set to 5 W/m².K in the early stage and increased to 10 W/m²·K from approximately 900s onward to represent stronger heat dissipation.

B3. Case B - Time-dependent CO_2 adsorption in ANSYS Fluent

Case B was solved on a 3D single-column model with a top inlet, a porous zeolite bed, and a bottom outlet. The inlet gas contained 15% CO_2 and the balance air at 300 K. The equilibrium behaviour was described with the Toth isotherm, whereas adsorption kinetics followed the LDF model. CO_2 in the gas phase was consumed through a sink term and the bed loading q was updated through the UDS variable in the porous region.

The simulated time for case B was 1800s. The exported outputs included the CO_2 mass-fraction contour at 1350s, gas-flow pathlines through the distributor chamber and the bed, and the breakthrough curve at the outlet. The initial condition corresponded to fresh zeolite, so the outlet concentration remained near zero until the adsorption front approached the outlet.

For case B, besides the breakthrough curve, the adsorption step is used to extract the CO_2 removal efficiency and the cumulative captured CO_2 inventory. The instantaneous removal efficiency is evaluated as $\eta_{rem} = 1 - \frac{y_{out}}{y_{in}}$, while the amount of CO_2 captured during the adsorption step is obtained from the breakthrough integral $m_{capt} = \int_0^{t_{sw}} \dot{m}_g (y_{in} - y_{out}) dt$. These adsorption-side quantities are later combined with the regenerated CO_2 amount from case C when discussing the overall recovery ratio and cycle-level SEC.

B3. Case C: Desorption/regeneration in ANSYS Fluent

Case C was formulated in a simplified way, but calibrated to the thermal trend obtained in case A. The zeolite bed was assumed to be uniformly saturated at the beginning of regeneration with UDS-0 ≈ 0,198, representing the mass of adsorbed CO_2 per unit mass of zeolite, while the gas phase in the void space was initialized with negligible CO_2. The column wall was heated and the outlet was defined as a pressure-outlet with negative gauge pressure to mimic mild vacuum regeneration.

No purge gas was introduced in order to avoid dilution of the regenerated CO_2 stream. Desorption was represented by a time-dependent source term based on effective loading, so that the bed exhibits an initial thermal lag followed by a stronger desorption stage once the coldest region has been sufficiently heated. The main monitored quantities were q-bed-avg versus time and the final scalar-0 contour at t = 1800s.

C. Results and discussion

C1. Results of case A in Transient Thermal

Figure 2 presents the evolution of three representative temperatures: maximum (green), average (blue), and minimum (red). The maximum temperature rises rapidly and reaches about 576,71 K shortly after the initial heating stage; it then remains almost constant until roughly 600s before gradually decreasing because of heat exchange with the surroundings. In contrast, the average temperature and especially the minimum temperature respond much more slowly, reflecting the thermal inertia of the column body and packed bed.

From the temperature history, the minimum temperature

at 120s is still only about 304,90 K, whereas the average temperature has already reached about 380,28 K. In the 600 - 800s range, the average temperature reaches its peak at approximately 515 K and the minimum temperature reaches a peak of about 496,75 K. At the final time of 1800s, the minimum, average, and maximum temperatures decrease to approximately 380,77 K, 392,43 K, and 415,05 K, respectively, showing that the whole system enters a cooling stage after substantial heat storage.

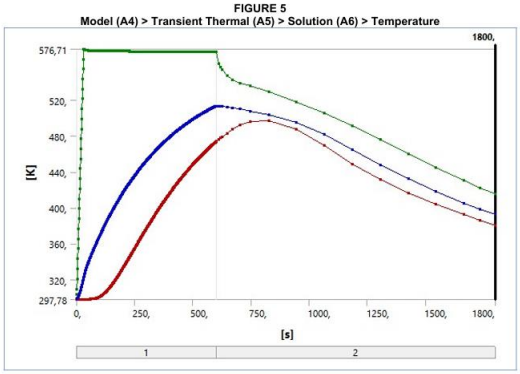


Figure 2. Evolution of maximum (green), average (blue), and minimum (red) temperatures in case A

These results have direct implications for regeneration design: the coldest region always lags significantly behind the heater temperature. Therefore, regeneration performance cannot be assessed only from the heater or wall-set temperature; the relevant design criterion must be the minimum temperature inside the zeolite bed, because that region controls the actual extent of desorption.

C2. Results and discussion for case B

At 1350s, the CO_2 mass-fraction contour shows that the gas near the upper inlet has already reached a high concentration, approximately 0,12 - 0,15, while the concentration decreases progressively along the axial direction and becomes very low near the outlet. This indicates that the adsorption front is still inside the packed bed: zeolite near the inlet has adsorbed more CO_2 and is close to saturation, whereas the lower part of the bed still retains strong capture capability.

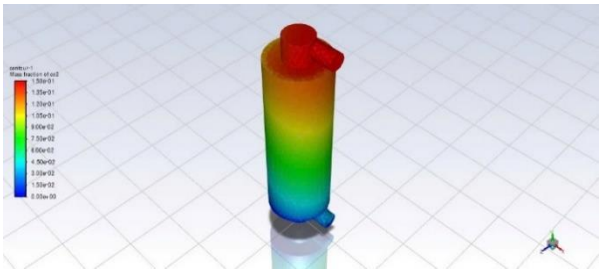


Figure 3. CO_2 mass-fraction contour in the bed at 1350s

The pathline plot shows that gas enters from the upper inlet, is redistributed in the top chamber, and then forms relatively uniform streamlines along the axial direction down to the outlet. Although local turning and mixing remain near the inlet mouth, the trajectories become much more regular once the flow enters the packed bed. This confirms that the current geometry provides an acceptable flow distribution and limits severe channeling.

The breakthrough curve shows that the outlet CO_2 concentration remains nearly zero during the early period and starts to increase significantly only after about 1350s. The rise becomes steep in the 1400–1750s interval, and by 1800s the outlet concentration reaches approximately 0,125, still lower than the inlet value of 0,15. This means that the mass-transfer zone has approached the outlet but has not completely left the column within the simulated time window.

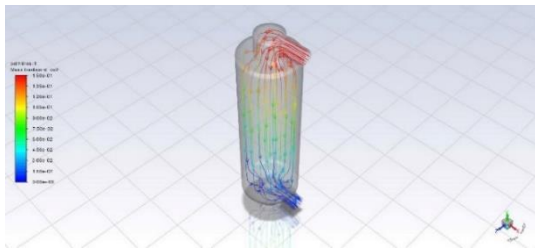


Figure 4. Gas pathlines through the bed at 1350s

From the viewpoint of dual-column TSA operation, these results suggest that column switching should be scheduled slightly before the steep breakthrough region, approximately in the 1300 -1400s range, so as to maintain clean-gas quality at the outlet while still utilizing the dynamic capacity of the zeolite bed. The consistency among the concentration contour, gas-flow pathlines, and the breakthrough curve confirms that case B captures the expected physical behaviour of a moving adsorption front in a packed bed.

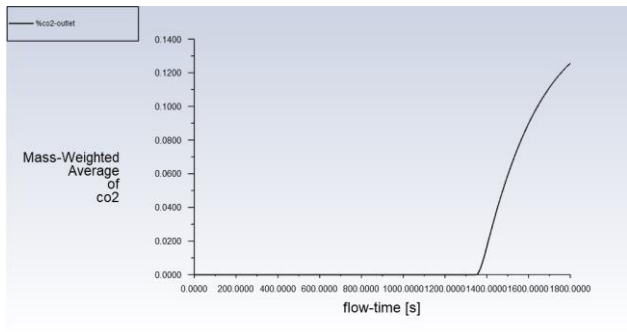


Figure 5. Breakthrough curve of outlet CO_2 concentration

For case B, with $y_{in} = 0{,}15$ and the simulated breakthrough curve, the outlet-removal efficiency remains close to 100% up to approximately 1350s because y_{out} is nearly zero during this interval. At the end of the simulated run, y_{out} is about 0,125, which corresponds to $\eta_{rem} \approx 1 - \frac{0.125}{0.15} \approx 16{,}7\%$. Therefore, the practically useful adsorption window for high-quality cleaned gas lies before the sharp breakthrough region, and the cumulative CO_2 captured up to the selected switching time provides the adsorption-side basis for the subsequent recovery analysis.

C3. Results and discussion for case C

The q-bed-avg curve shows that the average adsorption loading remains nearly unchanged during the initial thermal-lag period and then decreases most strongly in the 700 - 1300s

interval before approaching the residual value at the end of the cycle. This behaviour is consistent with case A: the bed requires a finite time for the coldest region to reach a sufficiently high temperature before desorption becomes dominant. By 1800s, q-bed-avg decreases from about 0,198 to near 0,005, indicating that most of the adsorbed CO_2 has been released from the zeolite bed.

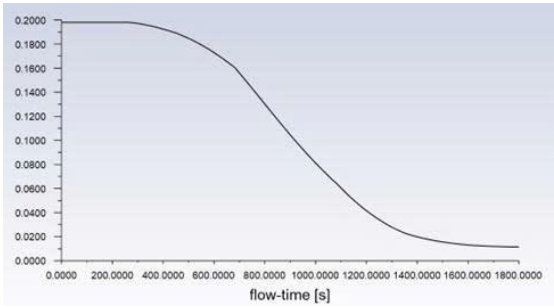


Figure 6. Time history of q-bed-avg during regeneration

The final scalar-0 contour indicates an almost uniform residual loading, on the order of $5{,}03\times10^{-3}$ to $5{,}07\times10^{-3}$ throughout the bed. This confirms that wall heating combined with outlet vacuum is capable of regenerating the zeolite layer relatively uniformly. Taken together with the q-bed-avg history, case C captures the three expected regeneration stages: initial thermal lag, dominant desorption in the middle stage, and gradual convergence toward the residual loading at the end of the cycle.

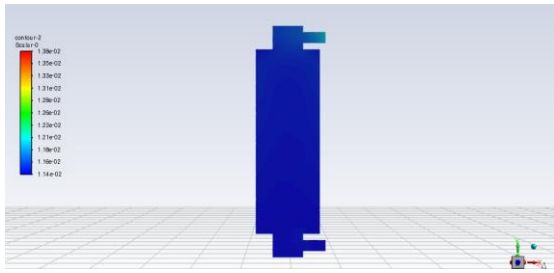


Figure 7. Final contour of the remaining CO_2 loading in the bed at t = 1800s

From the regeneration result, the bed-scale desorption ratio can be estimated as $R_{regen} = \frac{(0{,}198-0{,}005)}{0{,}198} \approx 97{,}5\%$, indicating that nearly all of the adsorbed CO_2 inventory is released during the 1800 s regeneration step. Because the present TPSA model imposes wall temperature as a thermal boundary rather than a detailed electrical heater-power model, a reliable SEC value in $\frac{kJ}{kg_{CO_2}}$ cannot yet be reported from simulation alone. Likewise, a single cycle-averaged CO_2 product purity requires time-integration of the outlet composition during desorption; in the present no-purge vacuum configuration, the regenerated stream is expected to be CO_2-rich, but the final purity value is reserved for experimental validation with an online gas analyser. In the prototype stage, these quantities will be evaluated from outlet composition and flow-rate data according to $Purity = \frac{n_{CO2,out}}{n_{total,out}}$, $Recovery = \frac{n_{CO2,recovered}}{n_{CO2,captured}}$, and $SEC = \frac{E_{regen}}{m_{CO2,recovered}}$.

ACKNOWLEDGEMENT

This research was supported by the University of Technology and Education – University of Danang under the student scientific research project code SV2026-23, according to Decision No.1111/QĐ-ĐHSPKT dated November 14, 2025, of the President of the University of Technology and Education.

REFERENCES

[1] U.S. Department of Energy, National Energy Technology Laboratory, "Carbon dioxide capture approaches," FE0013122.

[2] Intergovernmental Panel on Climate Change, IPCC Special Report on Carbon Dioxide Capture and Storage. Cambridge, U.K.: Cambridge University Press, 2005, ch. 3, "Capture of CO_2."

[3] BASF, "BASF 13X Molecular Sieve—Product Data Sheet [4] Micromeritics Instrument Corp., "CO_2 adsorption in zeolite 13X," Application Note 188.

[5] ANSYS, Inc., "Fluent User-Defined Function (UDF) manual: Detailed example UDFs," ANSYS Help System, ver. 25.2, 2025.

[6] M. Erguvan and S. Amini, "Parametric investigation of CO_2 desorption of zeolite 13X under microwave condition," Carbon Capture Science & Technology, vol. 11, Art. no. 100189, 2024, doi: 10.1016/j.ccst.2024.100189.

[7] K. Zabielska, T. Aleksandrzak, and E. Gabruś, "Adsorption equilibrium of carbon dioxide on zeolite 13X at high pressures," Chemical and Process Engineering, vol. 39, no. 3, pp. 309–321, 2018, doi: 10.24425/122952.

[8] S. Cavenati, C. A. Grande, and A. E. Rodrigues, "Adsorption equilibrium of methane, carbon dioxide, and nitrogen on zeolite 13X at high pressures," Journal of Chemical & Engineering Data, vol. 49, no. 4, pp. 1095–1101, 2004, doi: 10.1021/je0498917.

[9] S. Sircar and J. R. Hufton, "Why does the linear driving force model for adsorption kinetics work?" Adsorption, vol. 6, no. 2, pp. 137–147, Jun. 2000, doi: 10.1023/A:1008965317983.

[10] ANSYS, Inc., "Species transport equations," ANSYS Fluent Theory Guide, 2025.

[11] ANSYS, Inc., "Energy equation," ANSYS Fluent Theory Guide, ver. 24.2, 2024.

[12] ANSYS, Inc., "Cell zone conditions," ANSYS Fluent User's Guide, ver. 24.2, 2024.

[13] K. G. Allen, T. W. von Backström, and D. G. Kröger, "Packed bed pressure drop dependence on particle shape, size distribution, packing arrangement and roughness," Powder Technology, vol. 246, pp. 590–600, Sep. 2013, doi: 10.1016/j.powtec.2013.06.022.

[14] D. D. Do, Adsorption Analysis: Equilibria and Kinetics. London, U.K.: Imperial College Press, 1998.

[15] Q. P. Dang, T. T. Son, and C. H. Nguyen, *Heat*

Transfer. Hanoi: Vietnam Education Publishing House, 2008.

[16] E. Sonnleitner, G. Schöny, and H. Hofbauer, "Assessment of zeolite 13X and Lewatit® VP OC 1065 for application in a continuous temperature swing adsorption process for biogas upgrading," Biomass Conversion and Biorefinery, vol. 8, no. 2, pp. 379–395, 2018, doi: 10.1007/s13399-017-0293-3.

[17] F. Su and C. Lu, "CO2 capture from gas stream by zeolite 13X using a dual-column temperature/vacuum swing adsorption," Energy & Environmental Science, vol. 5, no. 10, pp. 9021–9027, 2012, doi: 10.1039/C2EE22647B.

[18] ANSYS, Inc., "Reading and writing case and data files," ANSYS Fluent User's Guide, ver. 25.2, 2025